Stabilities, Electronic Structures, and Bonding Properties of Iron Complexes $(E_1E_2)Fe(CO)_2(CNAr^{Tripp2})_2$ (E_1E_2 = BF, CO, N_2, CN^-, or NO^+)**

Gerui Pei,[a] Pei Zhao,[b, c] Song Xu,[a] Xintian Zhao,[a] Chuncai Kong,[a] Zhimao Yang,[a] Masahiro Ehara,*[b, c] and Tao Yang*[a]

The coordination of 10-electron diatomic ligands (BF, CO N_2) to iron complexes $Fe(CO)_2(CNAr^{Tripp2})_2$ [Ar^{Tripp2} = 2,6-(2,4,6-(*iso*-propyl)$_3C_6H_2)_2C_6H_3$] have been realized in experiments very recently (*Science*, **2019**, *363*, 1203–1205). Herein, the stability, electronic structures, and bonding properties of $(E_1E_2)Fe(CO)_2(CNAr^{Tripp2})_2$ (E_1E_2 = BF, CO, N_2, CN^-, NO^+) were studied using density functional (DFT) calculations. The ground state of all those molecules is singlet and the calculated geometries are in excellent agreement with the experimental values. The natural bond orbital analysis revealed that Fe is negatively charged while E_1 possesses positive charges. By employing the energy decomposition analysis, the bonding nature of the E_2E_1–$Fe(CO)_2(CNAr^{Tripp2})_2$ bond was disclosed to be the classic dative bond $E_2E_1 \rightarrow Fe(CO)_2(CNAr^{Tripp2})_2$ rather than the electron-sharing double bond. More interestingly, the bonding strength between BF and $Fe(CO)_2(CNAr^{Tripp2})_2$ is much stronger than that between CO (or N_2) and $Fe(CO)_2(CNAr^{Tripp2})_2$, which is ascribed to the better σ-donation and π back-donations. However, the orbital interactions in $CN^- \rightarrow Fe(CO)_2(CNAr^{Tripp2})_2$ and $NO^+ \rightarrow Fe(CO)_2(CNAr^{Tripp2})_2$ mainly come from σ-donation and π back-donation, respectively. The different contributions from σ donation and π donation for different ligands can be well explained by using the energy levels of E_1E_2 and $Fe(CO)_2(CNAr^{Tripp2})_2$ fragments.

1. Introduction

Carbon monoxide (CO), which is a diatomic molecule with 10 valence electrons, is among the most widely studied ligands in organometallic chemistry. Carbonyl complexes, especially the homoleptic carbonyl complexes, are prototypical examples of the Dewar–Chatt–Duncanson (DCD) model.[1,2] By using the DCD model, the bonding interaction between CO and transition metals could be mainly classified as two components, including σ-donation from the lone pair of CO to an empty orbital on the metal and π back-donation from occupied *d*-orbitals of the metal to the π^* orbitals of CO.[3] Although the former usually plays as a primary bonding interaction, π back-donations are important and sometimes are the dominant contribution in bonding interactions.[4,5] Several other 10-electron diatomic ligands are isoelectronic and isolobal to CO, including neutral ligands N_2 and BF and ionic ligands CN^-, and NO^+.[6] Compared with CO, N_2 has lower-energy σ-donor orbitals and higher-energy π^* orbitals, revealing its lower binding ability. Both CN^- and NO^+ are weak ligands because of less π-acceptor ability and σ-donor ability, respectively. The binding nature of N_2, CN^- and NO^+ to transition metals has been characterized experimentally and theoretically.[3,6]

The boron monofluoride (BF) has a decreased HOMO-LUMO gap (HOMO, highest occupied molecular orbital; LUMO, lowest unoccupied molecular orbital) compared to CO.[7] On one hand, the resulted in better σ-donor and π-acceptor abilities lead to more favorably ligating properties to transition metals. On the other hand, the small HOMO-LUMO gap gives rise to more reactivity and instability at room temperature.[8] Lots of efforts have been devoted to fluoroborylene complexes since Timms postulated the first fluoroborylene complex $[Fe(BF)(PF_3)_4]$ in 1973.[9–11] Braunschweig *et al.* detected the bridged fluoroborylene complex $[\{(OC)_5Mn\}_2(\mu\text{-BF})]$ by using ^{11}B NMR spectrum.[12] A synthesis and structural characterization of fluoroborylene ruthenium complex $Cp_2Ru_2(CO)_4(\mu\text{-BF})$, in which BF ligand is bridged between transition metal centers, were reported by Vidovic and Aldridge.[13,14] By using reactions of laser-ablated metal atoms with BF_3, Wang, Andrews, and co-workers synthesized terminal fluoroborylene complexes $FBMF_2$ (M = transition metal) in the gas phase.[15–17] Fluoroborylene iron carbonyls and

[a] G. Pei, S. Xu, X. Zhao, Prof. C. Kong, Prof. Z. Yang, Prof. T. Yang
MOE Key Laboratory for Nonequilibrium Synthesis and Modulation of Condensed Matter, School of Physics, Xi'an Jiaotong University
E-mail: taoyang1@xjtu.edu.cn
[b] Dr. P. Zhao, Prof. M. Ehara
Research Center for Computational Science
Institute for Molecular Science
Nishigonaka 38
Myodaiji, Okazaki 444-8585 (Japan)
E-mail: ehara@ims.ac.jp
[c] Dr. P. Zhao, Prof. M. Ehara
Elements Strategy Initiative for Catalysts and Batteries (ESICB)
Kyoto University
Kyoto 615-8520 (Japan)
E-mail: ehara@ims.ac.jp

[**] Ar^{Tripp2} = 2,6-(2,4,6-*iso*-propyl)$_3C_6H_2)_2C_6H_3$

Supporting information for this article is available on the WWW under https://doi.org/10.1002/open.202000248

homoleptic fluoroborylenes complexes have also been proposed theoretically by Hoffmann and Schaefer and King.[18–24]

Very recently, Figueroa *et al.* successfully realized the isolation of the iron complex $(BF)Fe(CO)_2(CNAr^{Tripp2})_2$ [Ar^{Tripp2} = 2,6-(2,4,6-(*iso*-propyl)$_3C_6H_2)_2C_6H_3$] with a terminal BF ligand, along with the isoelectronic dinitrogen and CO complexes $(N_2)Fe(CO)_2(CNAr^{Tripp2})_2$ and $Fe(CO)_3(CNAr^{Tripp2})_2$.[25] Further single-crystal x-ray diffraction, spectroscopic, and electron-density topology calculation studies demonstrated that the terminal BF ligand possesses particularly strong σ-donor and π-acceptor properties. However, the nature of the chemical bond could be altered from a dative bond to an electron-sharing double bond if the π-bonding interaction is strong enough. Therefore, the nature of B–Fe bond in $(BF)Fe(CO)_2(CNAr^{Tripp2})_2$ is unclear. Moreover, the σ-bonding interaction and π-bonding interaction strengths, which play as the dominant bonding interaction between Fe and BF, remain unknown.

In the present study, we report a theoretical study on geometries, electronic structures, and bonding properties of the 10-electron diatomic ligand to iron complexes $(E_1E_2)Fe(CO)_2(CNAr^{Tripp2})_2$ (E_1E_2 = BF, CO, N_2, CN^-, NO^+) by using DFT calculations. The nature of the Fe–E_1 bonds has been clarified. The bonding strengths of σ-interaction and π-interaction were analyzed and well explained by using the energy levels of 10-electron diatomic ligand.

2. Computational Methods

Test calculations on $(BF)Fe(CO)_2(CNAr^{Tripp2})_2$ by using BP86,[26,27] B3LYP,[28,29] BP86-D3(BJ),[30] and ωB97XD[31] functional with def2-SVP[32] basis set shows that both BP86 and ωB97XD could produce the experimental structure parameters well (please see ESI for details). Regarding the large calculation task in the present work, the BP86/def2-SVP was used to optimize all structures without any symmetry restriction. Frequency calculations were performed at the same level of theory to verify that all the structures are local minima. The functional dependence of the optimized structures and the spin states was examined as shown in Tables S1 and S2. The above DFT calculations were conducted using Gaussian 09 software.[33] The NBO[34] partial charges and Wiberg bond orders[35] were computed at BP86/def2-TZVPP[36] using NBO 3.1 as implemented in Gaussian 09.

The nature of the chemical bond E–Fe was investigated by means of an energy decomposition analysis (EDA) developed by Ziegler and Rauk.[37] The EDA focuses on the instantaneous interaction energy ΔE_{int} of a bond A–B between the fragments A and B in the particular electronic reference state at the frozen geometry of the molecule AB.[38–41] The interaction energy ΔE_{int} is divided into three main components [eqn (1)]. In the present calculations, the dispersion correction ΔE_{disp} term was also computed:

$$\Delta E_{int} = \Delta E_{elstat} + \Delta E_{Pauli} + \Delta E_{orb} \quad (1)$$

The term ΔE_{elstat} corresponds to the quasi-classical electrostatic interaction between the unperturbed charge distributions of the prepared atoms and is usually attractive. The Pauli repulsion ΔE_{Pauli} arises as the energy change associated with the transformation from the superposition of the unperturbed electron densities $\rho_A + \rho_B$ of the isolated fragments to the wavefunction $\Psi^0 = N\hat{A}[\Psi_A\Psi_b]$ which properly obeys the Pauli principle through explicit antisymmetrization ($\hat{A}$ operator) and renormalization (N = constant) of the product wavefunction. ΔE_{Pauli} comprises the destabilizing interactions between electrons of the same spin on either fragment. The orbital interaction ΔE_{orb} accounts for charge transfer, polarization effects, and electron-pair bonding. Finally, the dispersion interaction ΔE_{disp} is involved with the pairwise correction (DFT–D3) from Grimme.[30]

The EDA-NOCV[42,43] method combines the EDA with the natural orbitals for chemical valence (NOCV)[44–46] to decompose the orbital interaction term ΔE_{orb} into pairwise contributions. The NOCVs Ψ_i are defined as the eigenvector of the valence operator, V given by eqn (2).

$$\hat{V}\Psi_i = v_i\Psi_i \quad (2)$$

In the EDA-NOCV scheme the orbital interaction term, ΔE_{orb} is given by eqn (3),

$$\Delta E_{orb} = \sum_k \Delta E^k_{orb} = \sum_{k=1}^{\frac{N}{2}} v_k[-F^{TS}_{-k,-k} + F^{TS}_{k,k}] \quad (3)$$

in which $F^{TS}_{-k,-k}$ and $F^{TS}_{k,k}$ are diagonal transition state Kohn–Sham matrix elements corresponding to NOCVs with the eigenvalues $-v_k$ and v_k, respectively. The ΔE^k_{org} term for a particular type of bond is assigned by visual inspection of the shape of the deformation density $\Delta\rho_K$. The latter term is a measure of the size of the charge deformation and it provides a visual notion of the charge flow that is associated with the pairwise orbital interaction. The EDA-NOCV scheme thus provides both qualitative and quantitative information about the strength of orbital interactions in chemical bonds. The EDA-NOCV has been proven very useful for clarifying bond nature and analysing the σ-bonding and π-bonding interactions of various main-group compounds and transition metal complexes.[47–49]

The EDA-NOCV calculations were carried out with the program package ADF2019[50] with the zeroth-order regular approximation (ZORA) using DFT functional BP86 and Grimme's Beck-Johnson damping dispersion correction D3(BJ) with uncontracted Slater-type orbitals (STOs) with TZ2P+ quality as basis functions on the BP86/def2-SVP optimized geometries.

3. Results and Discussion

To determine the spin state of the $(E_1E_2)Fe(CO)_2(CNAr^{Tripp2})_2$ (E_1E_2 = BF, CO, N_2, CN^-, NO^+) compounds, the singlet and triplet states have been examined. As shown in Table 1, the singlet-

Table 1. The singlet-triplet splitting electronic energy $E_{S\text{-}T}$ and Gibbs free energy $G_{S\text{-}T}$ for $(E_1E_2)Fe(CO)_2(CNAr^{Tripp2})_2$ (E_1E_2 = BF, CO, N_2, CN^-, NO^+) given in kcal/mol.

E_1E_2	BF	CO	N_2	CN^-	NO^+
$E_{S\text{-}T}$	25.87	43.79	7.72[a]	32.99	28.81
$G_{S\text{-}T}$	24.27	40.87	2.93[a]	29.81	25.26

[a] The electronic energy and Gibbs free energy were calculated at the ωB97XD/def2-SVP level because BP86/def2-SVP met the serious convergence problem in calculating the triplet state.

triplet splitting energy values for all five compounds are positive. Except for $(N_2)Fe(CO)_2(CNAr^{Tripp2})_2$, the singlet state is more stable by over 24 kcal/mol than the triplet state. These results revealed that the ground state of five compounds is the singlet state. The calculations by using B3LYP and M06-L[51] also gave singlet as the ground state.

Two selected optimized geometric structures of $(BF)Fe(CO)_2(CNAr^{Tripp2})_2$ and $Fe(CO)_3(CNAr^{Tripp2})_2$ are shown in Figure 1, and the calculated and experimental bond length and bond angle values are presented in Table 2. It can be seen from Table 2 that the calculated results are in excellent agreement with the experimental values. The optimized structures of $(E_1E_2)Fe(CO)_2(CNAr^{Tripp2})_2$ (E_1E_2 = CO, N_2, NO^+) maintain the almost standard trigonal bipyramidal coordination geometries, as indicated by C1–Fe–C2 angles of 178.7°,177.9°and 171.8° for CO, N_2, and NO^+, respectively. However, the trigonal bipyramidal geometry in $(BF)Fe(CO)_2(CNAr^{Tripp2})_2$ has an obvious distortion and the C1-Fe–C2 bond angle is only 157.5°, which may come from the better σ-acceptor properties of BF.[18,20] The trigonal bipyramidal geometry in $[(CN)Fe(CO)_2(CNAr^{Tripp2})_2]^-$ has been obviously distorted, in which the bond angle of C1–Fe–C2 in is 144.3° while the C_N(equatorial) –Fe–C_O(equatorial) is as large as 167.6°. Besides, the E_1–E_2 bond in $(E_1E_2)Fe(CO)_2(CNAr^{Tripp2})_2$ is elongated moderately by about 0.02 Å with respect to the free E_1E_2 except for the distorted $[(NO)Fe(CO)_2(CNAr^{Tripp2})_2]^+$.

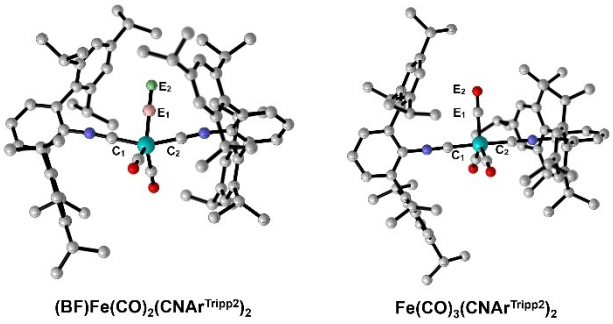

Figure 1. Optimized geometries of $(BF)Fe(CO)_2(CNAr^{Tripp2})_2$ and $Fe(CO)_3(CNAr^{Tripp2})_2$ at the BP86/def2-SVP level.

Table 2. Calculated and experimental results for selected bond length (L, in Å), bong angle (A, in degree), E_1–E_2 stretching wavenumbers (v, in cm^{-1}) of $(E_1E_2)Fe(CO)_2(CNAr^{Tripp2})_2$ (E_1E_2 = BF, CO, N_2, CN^-, NO^+) and isolated E_1E_2 ligand. The experimental data are from ref. 25.

E_1E_2		L (Fe–E_1)	L (E_1–E_2)	A (C1–Fe–C2)	*V* (E_1–E_2)
BF	Calc.	1.782	1.301	157.489	1401
	Expt.	1.770	1.277	160.378	1407
free BF	Calc.		1.277		1366
CO	Calc.	1.792	1.167	178.652	1972
	Expt.	1.809	1.144	178.606	1940
free CO	Calc.		1.142		2150
N_2	Calc.	1.868	1.130	177.945	2180
	Expt.	1.885	1.105	179.038	2194
free N_2	Calc.		1.112		2384
CN^-	Calc.	1.946	1.184	144.295	2127
free CN^-	Calc.		1.192		2081
NO^+	Calc.	1.679	1.156	171.809	1934
free NO^+	Calc.		1.077		2401

The calculated E_1–E_2 stretching wavenumbers are in conformity with the experimental data. Noteworthy, it has been proved that the BP86 could reproduce very well the C–O stretching mode in carbonyl complexes.[52] Table 3 presents the energy levels and gaps of HOMO-LUMO of five compounds. The HOMO-LUMO gaps are in the range of 2.38–2.77 eV for $(E_1E_2)Fe(CO)_2(CNAr^{Tripp2})_2$ (E_1E_2 = BF, CO, and N_2), and these large values suggest their high kinetic stabilities. Meanwhile, these three compounds also exhibit similar HOMO and LUMO energy levels. In contrast, the HOMO and LUMO energy levels for $[(CN)Fe(CO)_2(CNAr^{Tripp2})_2]^-$ are close to zero while those for $[(NO)Fe(CO)_2(CNAr^{Tripp2})_2]^+$ are much lower, which are attributed to their charged state. The small $gap_{HOMO\text{-}LUMO}$ also suggests their low kinetic stability. Figure 2 depicts the HOMOs and LUMO of $(BF)Fe(CO)_2(CNAr^{Tripp2})_2$. The HOMO and HOMO-1 mainly come from the Fe-3*d* orbital and B-2*p* orbital, whereas Fe-3*d* orbital, B-2*p* orbital, and N-2*p* orbital, as well as important contributions from the Tripp2 ligand, constitute the LUMO.

Table 4 shows the calculated NBO partial charges, the Wiberg bond orders P of selected atoms, and Fe–E_1 bond dissociation energy. $(E_1E_2)Fe(CO)_2(CNAr^{Tripp2})_2$ (E_1E_2 = BF, CO, CN^-) exhibit close bond dissociation energies ΔG_{BDE} in the range from +44.4 to +76.1 kcal/mol while a smaller value is identified for $(N_2)Fe(CO)_2(CNAr^{Tripp2})_2$. The $(NO)^+$–$Fe(CO)_2(CNAr^{Tripp2})_2$ bond is much stronger with the ΔG_{BDE} value of 147.5 kcal/mol. The ΔG_{BDE} calculations on the five complexes also reveal that all the substitution reactions are exothermic. For all five compounds,

Table 3. The energy levels (in eV) of HOMO and LUMO and HOMO-LUMO gap ($gap_{HOMO\text{-}LUMO}$, in eV) of $(E_1E_2)Fe(CO)_2(CNAr^{Tripp2})_2$ (E_1E_2 = BF, CO, N_2, CN^-, NO^+).

E_1E_2	BF	CO	N_2	CN^-	NO^+
LUMO	−2.49	−2.41	−2.42	+0.06	−6.63
HOMO	−5.22	−5.18	−4.80	−1.63	−7.98
$gap_{HOMO\text{-}LUMO}$	+2.73	+2.77	+2.38	+1.69	+1.35

Table 4. Calculated NBO partial charges q, Wiberg bond orders P, and Fe–E_1 bond dissociation energy (ΔG_{BDE}, in kcal/mol) in $(E_1E_2)Fe(CO)_2(CNAr^{Tripp2})_2$ (E_1E_2 = BF, CO, N_2, CN^-, NO^+).

E_1E_2	q (Fe)	q (E_1)	q (E_2)	P (Fe–E_1)	P (E_1–E_2)	ΔG_{BDE}
BF	−1.60	+1.04	−0.46	1.26	0.87	+66.5
CO	−1.40	+0.69	−0.45	1.25	2.07	+44.4
N_2	−1.12	+0.06	+0.02	0.79	2.70	+19.9
CN^-	−1.26	+0.25	−0.55	0.85	2.78	+76.1
NO^+	−1.04	+0.40	−0.07	1.49	1.97	+147.5

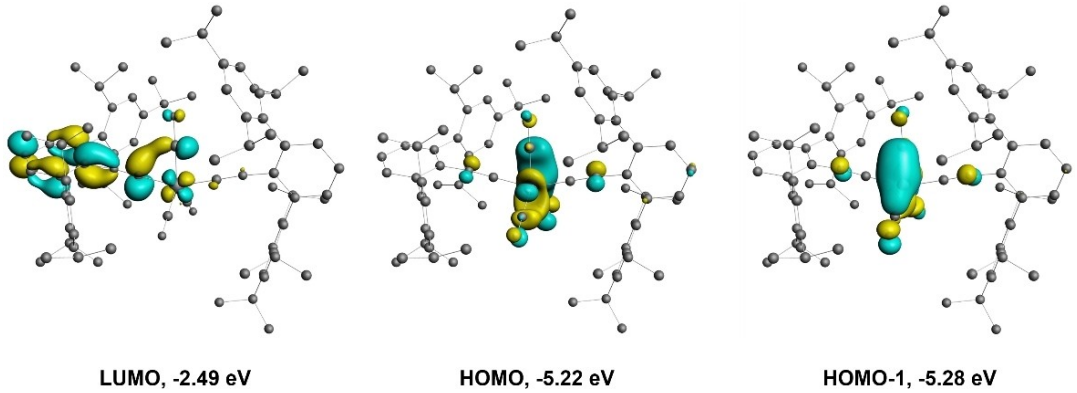

Figure 2. Plot of the unoccupied and occupied molecular orbitals of (BF)Fe(CO)$_2$(CNAr^{Tripp2})$_2$ at the BP86-D3(BJ)/TZ2P + level.

the iron atom carries negative charges ranging from −1.04 to −1.60. The E_1 is positively charged, whereas E_2 possesses a negative charge except for N_2. In particular, the boron atom in (BF)Fe(CO)$_2$(CNAr^{Tripp2})$_2$ has an obviously positive charge of +1.04, suggesting that the BF ligand has the strong ability of electron donation. The Wiberg bond orders of the Fe-E_1 bond range from 0.79 to 1.49, indicating that the Fe−E_1 is a single bond. However, the Wiberg bond orders of the E_1−E_2 bond are quite different. For BF, it is suggested that B–F is a single bond whereas N_2 and CN^- shown the bond orders range from 2.70 to 2.78, revealing triple bond character. In the case of CO and NO^+, the C–O and N–O bonds both are double bonds. To disclose more detailed information on the nature of the Fe–E_1 bonds in those five compounds, we carried out the EDA-NOCV calculations on (E_1E_2)Fe(CO)$_2$(CNAr^{Tripp2})$_2$ (E_1E_2 = BF, CO, N_2, CN^-, NO^+). Although five 10-electron diatomic ligands usually form a dative bond with transition metals, two bonding models including the dative bond and electron-sharing double bond have been analyzed, as shown in Scheme 1. The calculations for the dative bond use the neutral (or charged) singlet fragments E_1E_2 and the remaining neutral singlet fragment. In the case of the electron-sharing double bond, the neutral (or charged) triplet fragments E_1E_2 and triplet fragment were employed.

Table 5 presents the numerical EDA-NOCV results for all the five compounds (E_1E_2)Fe(CO)$_2$(CNAr^{Tripp2})$_2$ (E_1E_2 = BF, CO, N_2, CN^-, NO^+). The calculations revealed that the dative interactions E_2E_1→Fe are considered to be the best representation for the bonding situation in (E_1E_2)Fe(CO)$_2$(CNAr^{Tripp2})$_2$ because of the smaller absolute orbital interaction term ΔE_{orb} for the dative bond with respect to the electron-sharing double bond. The calculations suggest that the strength of the Fe-ligand interaction ΔE_{int} follows the order of $NO^+ > CN^- > BF > CO > N_2$.

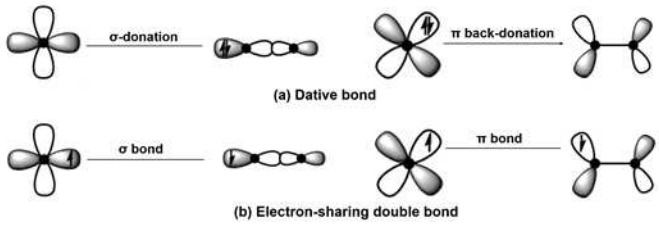

Scheme 1. Schematic representation for the two bonding models of the E_1–Fe bond in (E_1E_2)Fe(CO)$_2$(CNAr^{Tripp2})$_2$ (E_1E_2 = BF, CO, N_2, CN^-, NO^+).

For the three neutral ligands, it is found that the Fe-BF interaction strength is −81.6 kcal/mol, which is larger than the cases with CO and N_2. The covalent (orbital) interactions ΔE_{orb} and the Coulomb term ΔE_{elstat} have similar strengths for N_2 while ΔE_{elstat} is moderately stronger than ΔE_{orb} for BF and CO. The breakdown of ΔE_{orb} into the most important pairwise orbital interactions shows that the σ donation from BF to Fe fragment provides about 48.2% to the total orbital interactions while two π back-donations from the Fe fragment to BF π* contribute contributing about 40%. The σ donation from CO (or N_2) to Fe fragment is only about 33%–35%. However, the two π back-donations are stronger, which provides about 52%–54% to the total orbital interaction. Further examination on the energy values of σ interaction and π back-donations is stronger than that for CO and N_2, which agrees with the fact that BF has better σ-donation and π accepting properties than CO and N_2. Therefore, it is reasonable to conclude that the σ donation is more important than the π back-donations for BF–Fe interaction, whereas for CO–Fe and N_2-Fe interactions, showing the stronger π back-donations.

Although the charged ligand NO^+ and CN^- have stronger interaction strengths, the contributions from the main attractive interactions, ΔE_{elstat} and ΔE_{orb}, to the interaction strengths are quite different. As for CN^-, the electrostatic interaction ΔE_{elstat} is moderately larger than the orbital interaction ΔE_{orb}, in which the σ donation provides more than 60%. However, ΔE_{orb} plays a dominant role in the case of NO^+ and the π back-donations from Fe to NO^+ contribute about 79% to the total orbital interaction. These results agree well with the above Wiberg bond order results that the P (Fe–CN^-) is only 0.85 while the P (Fe–NO^+) is 1.49.

Figure 3 (a) shows the deformation density $\Delta\rho_1$ associated with the BF→Fe(CO)$_2$(CNAr^{Tripp2})$_2$ σ-donation. It comes from the σ lone pair orbital of the BF(*s*) ligand to the formally empty *d* orbitals of Fe(CO)$_2$(CNAr^{Tripp2})$_2$ with a large eigenvalue of ν = 0.98 and the stabilization energy of ΔE_{orb} = −71.1 kcal/mol. Two BF (π*)←Fe(CO)$_2$(CNAr^{Tripp2})$_2$ π back-donations are shown by the deformation density $\Delta\rho_2$ and $\Delta\rho_3$ in Figure 3 (b) and (c), both

Table 5. EDA-NOCV results of the E_2E_1–$Fe(CO)_2(CNAr^{Tripp2})_2$ bond in $(E_1E_2)Fe(CO)_2(CNAr^{Tripp2})_2$ (E_1E_2 = BF, CO, N_2, CN^-, NO^+) at the BP86-D3(BJ)/TZ2P+ level using different fragments. All values are in kcal/mol. The smallest ΔE_{orb} values for each species are indicated in bold.

	BF	CO	N_2	CN^-	NO^+
Dative bond with (singlet) and $Fe(CO)_2(CNAr^{Tripp2})_2$ (singlet)					
ΔE_{int}	−81.6	−58.3	−34.3	−93.3	−178.0
ΔE_{Pauli}	+273.3	+165.1	+99.4	+153.8	+137.5
ΔE_{disp}	−9.3	−8.2	−8.9	−10.9	−7.3
ΔE_{elstat} [a]	−198.2 (57.4%)	−119.0 (55.3%)	−62.7 (50.3%)	−132.1 (55.9%)	−49.5 (16.1%)
ΔE_{orb} [a]	−147.4 (42.6%)	−96.2 (44.7%)	−62.1 (49.7%)	−104.2 (44.1%)	−258.8 (83.9%)
$\Delta E_{orb(1)}$ [b] $E_1 \rightarrow Fe$ σ donation	−71.1 (48.2%)	−31.7 (33.0%)	−21.9 (35.3%)	−64.5 (61.9%)	−14.8 (5.7%)
$\Delta E_{orb(2)}$ [b] $E_1 \leftarrow Fe$ π back-donation	−37.1 (25.2%)	−31.7 (33.0%)	−19.7 (31.7%)	−7.8 (7.5%)	−131.3 (50.8%)
$\Delta E_{orb(3)}$ [b] $E_1 \leftarrow Fe$ π back-donation	−22.0 (15.0%)	−20.3 (21.1%)	−12.4 (20.1%)	−5.9 (5.7%)	−73.0 (28.2%)
$\Delta E_{orb(rest)}$ [b]	−17.2 (11.6%)	−12.5 (12.9%)	−8.1 (12.9%)	−26.0 (24.9%)	−39.7 (15.3%)
Electron-sharing double bond with E_1E_2 (triplet) and $Fe(CO)_2(CNAr^{Tripp2})_2$ (triplet)					
ΔE_{int}	−158.6	−209.1	−216.6	−227.0	−339.3
ΔE_{Pauli}	+181.1	+140.3	+128.1	+154.3	+169.4
ΔE_{disp}	−9.3	−8.2	−8.9	−10.9	−7.3
ΔE_{elstat} [a]	−142.2 (43.0%)	−104.1 (30.5%)	−80.8 (24.1%)	−108.0 (29.2%)	−87.2 (17.4%)
ΔE_{orb} [a]	−188.2 (57.0%)	−237.1 (69.5%)	−255.0 (75.9%)	−262.5 (70.8%)	−414.2 (82.6%)
$\Delta E_{orb(1)}$ [b] E_1–Fe σ bond	−87.1 (46.3%)	−138.6 (58.4%)	−177.3 (69.5%)	−95.2 (36.3%)	−261.2 (63.1%)
$\Delta E_{orb(2)}$ [b] E_1–Fe π bond	−67.9 (36.1%)	−69.8 (29.4%)	−57.4 (22.5%)	−139.6 (53.2%)	−50.8 (12.3%)
$\Delta E_{orb(rest)}$ [b]	−33.2 (17.6%)	−28.8 (12.2%)	−20.3 (8.0%)	−27.6 (10.5%)	−102.2 (24.6%)

[a] The values in parentheses give the percentage contribution to the total attractive interactions $\Delta E_{elstat} + \Delta E_{orb}$. [b] The values in parentheses give the percentage contribution to the total orbital interactions ΔE_{orb}.

from the doubly occupied orbitals in $Fe(CO)_2(CNAr^{Tripp2})_2$ get into the formally empty π^* orbitals of the BF ligand. The charge transfer along with π back-donations is relatively smaller of 0.70 and 0.41. While the σ-donation from the singly occupied orbital in CO(*s*) ligand into the formally empty *d* orbitals of $Fe(CO)_2(CNAr^{Tripp2})_2$, $CO(\sigma) \rightarrow Fe(CO)_2(CNAr^{Tripp2})_2$, is −31.7 kcal/mol with the charge flow $\nu_1 = 0.63$, as depicted in Figure 3 (d). The $\Delta\rho_2$ and $\Delta\rho_3$ in Figure 3 (e) and (f) show that the CO $\pi^*(p) \leftarrow Fe(CO)_2(CNAr^{Tripp2})_2$ π back-donations that come from the doubly occupied orbital in $Fe(CO)_2(CNAr^{Tripp2})_2$ into the formally empty $\pi^*(p)$ orbitals of the CO ligands. As shown in Figure S2 (g), (h) and (i), the shapes of deformation densities in $(N_2)Fe(CO)_2(CNAr^{Tripp2})_2$ are analogous to $Fe(CO)_3(CNAr^{Tripp2})_2$. The deformation densities $\Delta\rho_{1\text{-}3}$ of $(E_1E_2)Fe(CO)_2(CNAr^{Tripp2})_2$ (E_1E_2 = CN^-, NO^+) are depicted in Figure S2 (j) ~ (o).

To further explain the different contributions from σ donation and π back-donations for different ligands, we calculated the energy levels of E_1E_2 and $Fe(CO)_2(CNAr^{Tripp2})_2$ fragments in their deformed configurations, as shown in Table 6. For the three neutral ligands, the HOMO energy levels of E_1E_2 fragment are quite different and follow the order of BF > CO > N_2. However, the LUMO energy level of E_1E_2 fragment and

Table 6. The energy levels (eV) of HOMO and LUMO of E_1E_2 and $Fe(CO)_2(CNAr^{Tripp2})_2$ fragments of (E_1E_2 = BF, CO, N_2, CN^-, NO^+).

Ligand	E_1E_2 fragment		$Fe(CO)_2(CNAr^{Tripp2})_2$ fragment	
	HOMO	LUMO	HOMO	LUMO
BF	−6.98	−2.35	−4.17	−3.91
CO	−9.23	−2.41	−4.18	−3.28
N_2	−10.21	−2.30	−4.26	−3.22
CN^-	+0.55	+6.94	−4.52	−4.27
NO^+	−23.12	−15.62	−3.80	−3.04

HOMO and LUMO energy levels of $Fe(CO)_2(CNAr^{Tripp2})_2$ are close. Thus, the energy gap between $HOMO_{E_1E_2}$ and $LUMO_{Fe-fragment}$ follows the order of BF < CO < N_2, indicating that the strength of σ donation adopts the order of BF > CO > N_2, in agreement with the above EDA-NOCV results. Both HOMO and LUMO energy levels of the charged CN^- fragment are higher than zero and the σ donation should be much stronger than π back-donations, in conformity with the above results that the σ donation and π back-donations provide about 62% and 13.2% to the total orbital interactions, respectively. In contrast, the lower HOMO and LUMO levels for the negatively charged NO^+ suggest that the $LUMO_{NO^+}$ – $HOMO_{Fe-fragment}$ interaction is important, agreeing with the strong π back-donations from Fe $(CO)_2(CNAr^{Tripp2})_2$ fragment to NO^+, as shown in Table 6.

4. Conclusion

The stability, electronic structures, and bonding properties of T $(E_1E_2)Fe(CO)_2(CNAr^{Tripp2})_2$ (E_1E_2 = BF, CO, N_2, CN^-, NO^+) have been studied using density functional calculations. All those molecules have a singlet ground state. NBO analysis revealed that Fe is negatively charged while E_1 possesses positive charges. By employing the energy decomposition analysis, the binding nature of the E_2E_1–$Fe(CO)_2(CNAr^{Tripp2})_2$ bond was disclosed to be the classic dative bond $E_2E_1 \rightarrow Fe(CO)_2(CNAr^{Tripp2})_2$ rather than the electron-sharing double bond. The bonding strength between BF and $Fe(CO)_2(CNAr^{Tripp2})_2$ is much stronger than that between CO (or N_2) and $Fe(CO)_2(CNAr^{Tripp2})_2$, which comes from the better σ-donation and π back-donations. Thus, it can be sketched with the Lewis structure FB⋮⟹$Fe(CO)_2(CNAr^{Tripp2})_2$ because of the obvious π back-donations. However, the orbital interactions in $CN^- \rightarrow Fe(CO)_2(CNAr^{Tripp2})_2$ and $NO^+ \rightarrow Fe(CO)_2(CNAr^{Tripp2})_2$ mainly comes from σ-donation and π back-donations, respectively. The different contributions from σ donation and π donation for different ligands were well explained by using the energy levels of E_1E_2 and $Fe(CO)_2(CNAr^{Tripp2})_2$ fragments.

Acknowledgements

This work was supported by the National Natural Science Foundation of China (22003048, U1866203, 11674263), China Postdoctoral Science Foundation (2019 M663690), National Natural Science Foundation of Shaanxi Province (2020JZ-03), the Fundamental Research Funds for the Central Universities and the

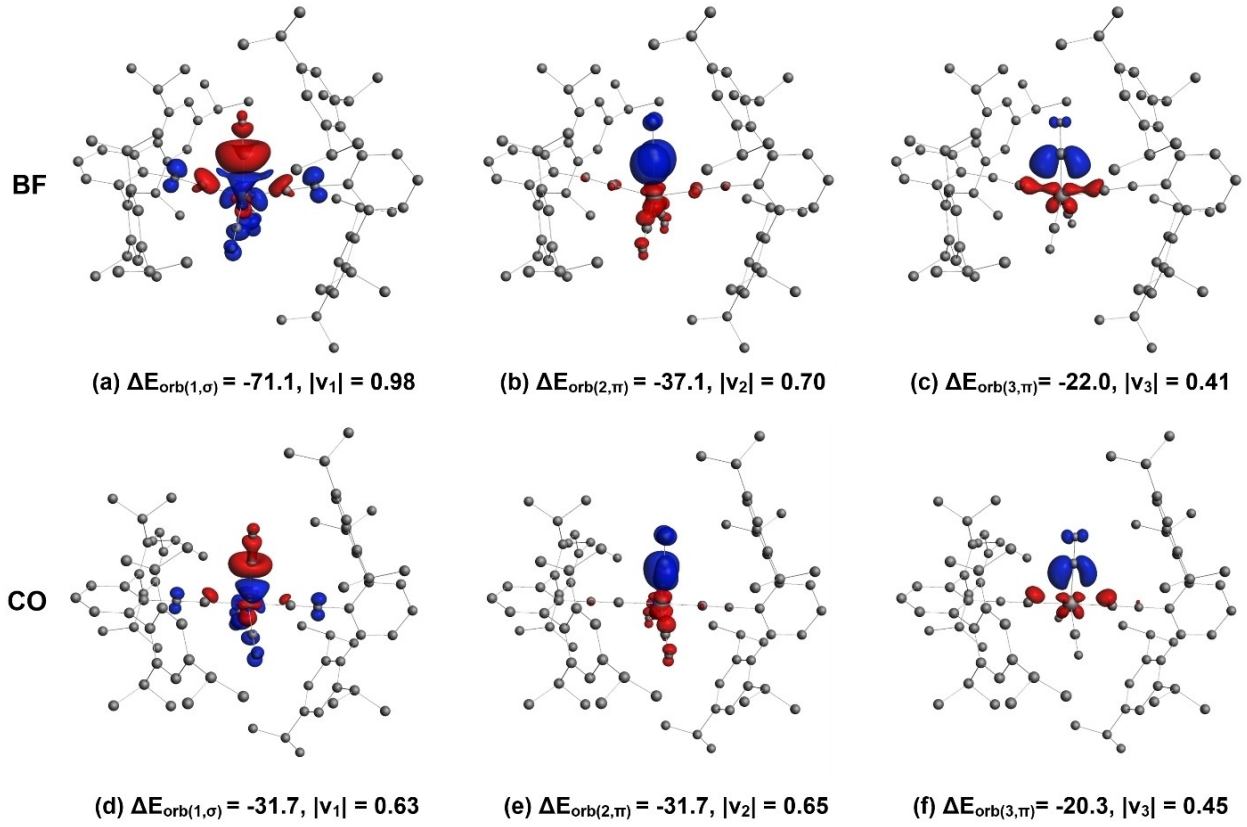

Figure 3. Plot of deformation densities $\Delta\rho_{1\text{-}3}$ (isovalue = 0.004) of the pairwise orbital interactions in $(E_1E_2)Fe(CO)_2(CNAr^{Tripp2})_2$ (E_1E_2 = BF, CO) at BP86-D3(BJ)/TZ2P+ level. The charge flow of the electronic charge is red→blue. The associated orbital interaction energies ΔE_{orb} are given in kcal/mol. The eigenvalues ν indicate the size of the charge flow.

World-Class Universities (Disciplines), and the Characteristic Development Guidance Funds for the Central Universities. M.E. acknowledges the financial support from a Grant-in-Aid for Scientific Research from the Japan Society for the Promotion of Science (JSPS) (JP16H06511, JP20H02718), Nanotechnology Platform Program (Molecule and Material Synthesis) of the Ministry of Education, Culture, Sports, Science, and Technology (MEXT) of Japan. DFT calculations were partially performed at the Research Center for Computational Science, Okazaki, Japan.

Conflict of Interest

The authors declare no conflict of interest.

Keywords: σ-donation/π back-donation · DCD model · density functional calculations · fluoroborylene complexes · iron complexes

[1] M. J. S. Dewar, *Bull. Soc. Chim. Fr.* **1951**, *18*, C71-C79.
[2] J. Chatt, L. Duncanson, *J. Chem. Soc.* **1953**, 2939–2947.
[3] A. W. Ehlers, S. Dapprich, S. F. Vyboishchikov, G. Frenking, *Organometallics* **1996**, *15*, 105–117.
[4] Y. Chen, K. Xin, J. Jin, W. Li, Q. Wang, X. Wang, G. Wang, *Phys. Chem. Chem. Phys.* **2019**, *21*, 6743–6749.
[5] X. Wu, L. Zhao, J. Jin, S. Pan, W. Li, X. Jin, G. Wang, M. Zhou, G. Frenking, *Science* **2018**, *361*, 912–916.
[6] H. Werner, *Chem. Int. Ed. Engl.* **1990**, *29*, 1077–1089.
[7] A. W. Ehlers, E. J. Baerends, F. M. Bickelhaupt, U. Radius, *Chem. Eur. J.* **1998**, *4*, 210–221.
[8] Y. Bu, M. Zhao, Y. He, W. Gao, Q. Jiang, *ChemPhysChem.* **2016**, *17*, 2998–3003.
[9] P. Timms, *J. Am. Chem. Soc.* **1967**, *89*, 1629–1632.
[10] P. Timms, *J. Am. Chem. Soc.* **1968**, *90*, 4585–4589.
[11] P. L. Timms, *Acc. Chem. Res.* **1973**, *6*, 118–123.
[12] H. Braunschweig, K. Kraft, T. Kupfer, K. Radacki, F. Seeler, *Angew. Chem. Int. Ed.* **2008**, *47*, 4931–4933; *Angew. Chem.* **2008**, *120*, 5009–5011.
[13] D. Vidovic, S. Aldridge, *Angew. Chem. Int. Ed. Engl.* **2009**, *48*, 3669–3672.
[14] H. Braunschweig, R. D. Dewhurst, *Angew. Chem. Int. Ed.* **2010**, *49*, 3412–3414; *Angew. Chem.* **2010**, *122*, 3486–3488.
[15] X. Wang, B. O. Roos, L. Andrews, *Angew. Chem. Int. Ed.* **2010**, *122*, 161–164.
[16] X. Wang, B. O. Roos, L. Andrews, *Chem. Commun.* **2010**, *46*, 1646–1648.
[17] B. Xu, W. Li, Z. Pu, W. Yu, T. Huang, J. Cheng, X. Wang, *Phys. Chem. Chem. Phys.* **2019**, *21*, 25577–25583.
[18] U. Radius, F. M. Bickelhaupt, A. W. Ehlers, N. Goldberg, R. Hoffmann, *Inorg. Chem.* **1998**, *37*, 1080–1090.
[19] L. Xu, Q.-s. Li, Y. Xie, R. B. King, H. F. Schaefer III, *New J. Chem.* **2010**, *34*, 2813–2821.
[20] L. Xu, Q.-s. Li, Y. Xie, R. B. King, H. F. Schaefer III, *Inorg. Chem.* **2010**, *49*, 1046–1055.
[21] L. Xu, Q.-s. Li, Y. Xie, R. B. King, H. F. Schaefer III, *Inorg. Chem.* **2010**, *49*, 2996–3001.
[22] L. Xu, Q.-s. Li, Y. Xie, R. B. King, H. F. Schaefer III, *Inorg. Chim. Acta* **2010**, *363*, 3538–3549.
[23] L. Xu, Q.-s. Li, R. B. King, H. F. Schaefer, *Organometallics* **2011**, *30*, 5084–5087.
[24] L. Xu, Q.-s. Li, R. B. King, *New J. Chem.* **2019**, *43*, 8220–8228.

[25] M. J. Drance, J. D. Sears, A. M. Mrse, C. E. Moore, A. L. Rheingold, M. L. Neidig, J. S. Figueroa, *Science* **2019**, *363*, 1203–1205.
[26] J. P. Perdew, *Phys. Rev. B: Condens. Matter. Phys.* **1986**, *33*, 8822.
[27] A. D. Becke, *Phys. Rev. A* **1988**, *38*, 3098–3100.
[28] A. D. Becke, *J. Chem. Phys.* **1993**, *98*, 5648–5652.
[29] P. J. Stephens, F. J. Devlin, C. F. Chabalowski, M. J. Frisch, *J. Phys. Chem.* **1994**, *98*, 11623–11627.
[30] S. Grimme, J. Antony, S. Ehrlich, H. Krieg, *J. Chem. Phys.* **2010**, *132*, 154104.
[31] J.-D. Chai, M. Head-Gordon, *Phys. Chem. Chem. Phys.* **2008**, *10*, 6615–6620.
[32] A. Schäfer, H. Horn, R. Ahlrichs, *J. Chem. Phys.* **1992**, *97*, 2571–2577.
[33] G. W. T. M. J. Frisch, H. B. Schlegel, G. E. Scuseria, M. A. Robb, J. R. Cheeseman, G. Scalmani, V. Barone, B. Mennucci, G. A. Petersson, H. Nakatsuji, M. Caricato, X. Li, H. P. Hratchian, A. F. Izmaylov, J. Bloino, G. Zheng, J. L. Sonnenberg, M. Hada, M. Ehara, K. Toyota, R. Fukuda, J. Hasegawa, M. Ishida, T. Nakajima, Y. Honda, O. Kitao, H. Nakai, T. Vreven, J. A. Montgomery, Jr., J. E. Peralta, F. Ogliaro, M. Bearpark, J. J. Heyd, E. Brothers, K. N. Kudin, V. N. Staroverov, T. Keith, R. Kobayashi, J. Normand, K. Raghavachari, A. Rendell, J. C. Burant, S. S. Iyengar, J. Tomasi, M. Cossi, N. Rega, J. M. Millam, M. Klene, J. E. Knox, J. B. Cross, V. Bakken, C. Adamo, J. Jaramillo, R. Gomperts, R. E. Stratmann, O. Yazyev, A. J. Austin, R. Cammi, C. Pomelli, J. W. Ochterski, R. L. Martin, K. Morokuma, V. G. Zakrzewski, G. A. Voth, P. Salvador, J. J. Dannenberg, S. Dapprich, A. D. Daniels, O. Farkas, J. B. Foresman, J. V. Ortiz, J. Cioslowski, D. J. Fox, **2013**.
[34] F. Weinhold, C. Landis, *Valency and Bonding: A Natural Bond Orbital Donor-Acceptor Perspective.*, Cambridge: Cambridge University Press, Cambridge: Cambridge University Press **2005**.
[35] K. B. Wiberg, *Tetrahedron* **1968**, *24*, 1083–1096.
[36] F. Weigend, R. Ahlrichs, *Phys. Chem. Chem. Phys.* **2005**, *7*, 3297–3305.
[37] T. Ziegler, A. Rauk, *Inorg. Chem.* **1979**, *18*, 1755–1759.
[38] F. M. Bickelhaupt, E. J. Baerends, *Rev. Comput. Chem.* **2000**, *15*, 1–86.
[39] G. t. Te Velde, F. M. Bickelhaupt, E. J. Baerends, C. Fonseca Guerra, S. J. van Gisbergen, J. G. Snijders, T. Ziegler, *J. Comput. Chem.* **2001**, *22*, 931–967.
[40] M. v. Hopffgarten, G. Frenking, *Wiley Interdiscip. Rev.: Comput. Mol. Sci.* **2012**, *2*, 43–62.
[41] P. Jerabek, H. W. Roesky, G. Bertrand, G. Frenking, *J. Am. Chem. Soc.* **2014**, *136*, 17123–17135.
[42] A. Michalak, M. Mitoraj, T. Ziegler, *J. Phys. Chem. A* **2008**, *112*, 1933–1939.
[43] M. P. Mitoraj, A. Michalak, T. Ziegler, *J. Chem. Theory Comput.* **2009**, *5*, 962–975.
[44] M. Mitoraj, A. Michalak, *J. Mol. Model.* **2007**, *13*, 347–355.
[45] M. Mitoraj, A. Michalak, *J. Mol. Model.* **2008**, *14*, 681–687.
[46] M. Mitoraj, A. Michalak, *Organometallics* **2007**, *26*, 6576–6580.
[47] L. Zhao, M. von Hopffgarten, D. M. Andrada, G. Frenking, *WIREs Comput. Mol. Sci.* **2018**, *8.* p. e1345.
[48] L. Zhao, S. Pan, N. Holzmann, P. Schwerdtfeger, G. Frenking, *Chem. Rev.* **2019**, *119*, 8781–8845.
[49] J. Jin, T. Yang, K. Xin, G. Wang, X. Jin, M. Zhou, G. Frenking, *Angew. Chem. Int. Ed.* **2018**, *57*, 6236–6241; *Angew. Chem.* **2018**, *130*, 6344–6349.
[50] *Computer code* ADF **2019**, SCM, Theoretical Chemistry, Vrije Universiteit, Amsterdam, the Netherlands. URL: *http://www. scm. com*.
[51] Y. Zhao, D. G. Truhlar, *J. Chem. Phys.* **2006**, *125*, 194101.
[52] R. K. Szilagyi, G. Frenking, *Organometallics* **1997**, *16*, 4807–4815.

Manuscript received: August 28, 2020
Revised manuscript received: October 7, 2020